An experimental investigation of the collective oscillations of bubble plumes entrained by breaking waves

M. R. Loewen[a)] and W. K. Melville[b)]
R.M. Parsons Laboratory, Department of Civil Engineering, Massachusetts Institute of Technology, Cambridge, Massachusetts 02139

(Received 17 April 1992; revised 20 September 1993; accepted 12 October 1993)

Laboratory measurements of the sound produced by mechanically generated two-dimensional (2-D) and three-dimensional (3-D) breaking waves are presented. In the 2-D breaking experiments it was observed that the mean-square pressure at frequencies below 1 kHz correlated strongly with the fractional energy dissipated by breaking and the volume of air entrained. In addition, the volume of air entrained was found to be proportional to the fractional energy dissipated. These results imply that measurements of the low-frequency sound may be useful for studying the dynamics of breaking waves in the field. It was found that 2-D plunging breakers produced significant increases in spectral levels at frequencies below approximately 500 Hz but that spilling breakers did not. Large-amplitude low-frequency signals were observed to begin up to $\frac{1}{3}$ of a wave period after the start of active breaking in both the two- and three-dimensional experiments. It is believed that these signals were due to the collective oscillation of the entrained bubble plumes. A model of a cylindrically shaped plume located immediately below the free surface and the void-fraction measurements of Lamarre and Melville [J. Acoust. Soc. Am. **95**, 1317–1328 (1994)] were used to compute the eigenfrequencies of the volume mode of collective oscillation. The computed eigenfrequencies closely matched the frequencies of the observed signals. This agreement between the experimental observations and theory provides considerable support for the hypothesis that the observed bubble plumes were oscillating collectively in their volume mode. This leads to the conclusion that the collective volume oscillations of bubble plumes entrained by breaking waves may be a source of low-frequency sound in the ocean.

PACS numbers: 43.30.Pc, 43.30.Ft, 43.30.Lz, 43.30.Nb

INTRODUCTION

Field experiments have shown that breaking waves generate sound at frequencies from 40 Hz to 20 kHz.[1–3] A number of experimental and analytic studies have provided convincing evidence that the dominant source of sound generated by breaking waves at frequencies greater than approximately 500 Hz is the oscillation of newly formed air bubbles at their linear resonant frequency.[4–8] Laboratory and field measurements beneath small-scale gently breaking waves have shown that the acoustic signals are composed of damped sinusoidal pulses with observed damping rates closely matching the theoretically predicted damping rates of air bubbles in water. The sound spectra of the laboratory and field data both had slopes of approximately −5 dB per octave at frequencies greater than 1 kHz, in agreement with the well-known Knudsen spectra.[5,8,9] From these results it was concluded that the source of the Knudsen sound spectra beneath gently breaking waves is the oscillation of newly created air bubbles entrained by breaking waves.

Papanicolaou and Raichlen[10] conducted an exploratory laboratory investigation of the sound produced by mechanically generated breaking waves. They found that plunging breakers produced sound at frequencies as low as 100 Hz and that the higher-frequency sound generated by breaking was similar for spilling and plunging events. They speculated that the observed low-frequency signals may be due to collective oscillations of the bubble plumes.

Others had suggested that the collective oscillation of bubble plumes entrained by breaking waves may be an important source of sea surface sound at frequencies below 500 Hz.[11,12] Prosperetti[11] postulated that a plume of bubbles could behave like a system of coupled oscillators, pulsating at a much lower frequency than the resonant frequency of the individual bubbles. Carey *et al.*[12] derived an expression for the frequency of the lowest mode of oscillation (lowest eigenfrequency) of a spherically shaped bubble plume,

$$f_0=(1/2\pi r_0)\sqrt{3\gamma P_0/(\rho\bar{\alpha})}, \tag{1}$$

where r_0 is the radius of the plume, γ is the ratio of the specific heats, ρ is the density of water, P_0 is the equilibrium pressure inside the individual bubbles, and $\bar{\alpha}$ is the mean void fraction within the plume.[12] For bubble plumes oscillating collectively, isothermal conditions apply and $\gamma=1$. For example, Eq. (1) predicts that a spherical bubble plume with radius, $r_0=0.3$ m, mean void fraction, $\bar{\alpha}=0.1$ and $P_0=101$ kPa would radiate sound at 30 Hz.

[a)]Present address: The Department of Mechanical Engineering, University of Toronto, Toronto, Ontario M5S 1A4, Canada.
[b)]Present address: Scripps Institution of Oceanography, University of California San Diego, La Jolla, CA 92093-0213.

Two recent laboratory studies have provided experimental evidence that bubble plumes generate sound by collectively oscillating.[13,14] Yoon *et al.*[13] conducted an experimental investigation of the collective oscillations of a cylindrical bubble column. The column was generated by the steady injection of air through a series of hypodermic needles located at the bottom of a tank of fresh water. The measured acoustic spectra showed low-frequency peaks from 260 to 550 Hz. Lu *et al.*[15] used averaged equations to calculate the eigenfrequencies of cylindrical bubble column based on the assumption that the bubbly air–water mixture is a continuum described by effective bulk properties. Yoon *et al.*[13] compared the observed frequencies to theoretically predicted values using the results of Lu *et al.*[15] The agreement between the experimental and theoretical results was excellent. They concluded that their results support the hypothesis that most of the observed oceanic ambient sound at frequencies below 1 kHz may be due to the collective oscillation of bubble plumes produced by breaking waves.

Kolaini *et al.*[14] studied the sound generated by bubble plumes produced when a fixed cylindrical volume of water is dropped onto a still water surface. The characteristics of the bubble plume were varied by changing the height from which the cylinder of water was dropped and by changing the volume of water dropped. They found that the frequency generated when a substructure detaches from the rest of the plume correlated with the volume of water that was dropped. The detached substructures were observed to oscillate at frequencies as low as tens of Hz. Their observations suggested that the substructures were spherical regions of high void fraction with a region of pure water positioned near the center. They found that if the void fraction within the substructures was assumed to be approximately 40% then estimates of the lowest eigenfrequency based on the observed plume size agreed with the observed frequencies. However, this experiment is far removed from the oceanic problem.

Our primary motivation for conducting this research was to investigate whether passive acoustic measurements could be used to obtain information on the dynamics of breaking waves. This required that we generate energetic spilling and plunging breaking waves in a physically realistic manner. The only methods we are aware of which meet this criterion involve the mechanical generation of waves in channels or basins. Therefore we have conducted the experiments described here in laboratory wave tanks. The finite size of the wave tanks and the long wavelengths of the observed acoustic signals forced us to position the hydrophones in the acoustic near field of the breaking waves. This means that we have, in fact, measured the near-field pressure fluctuations beneath breaking waves and that the observed signals may contain contributions from both the propagating and nonpropagating pressure fields. However, we will present convincing evidence that we have observed low-frequency pressure signals which are generated by the collective volume oscillations of the bubble plumes.

We present results from two series of experiments in which the near-field pressure fluctuations generated by controlled repeatable 2-D (two-dimensional) and 3-D (three-dimensional) breaking waves were measured. Low-frequency signals were observed beneath both the 2-D and 3-D breaking waves and large amplitude spectral peaks were observed at frequencies as low as 30 Hz. The observed frequencies are compared to theoretically predicted estimates of the lowest eigenfrequency (volume mode) of a semicircular bubble plume located at the free surface. Lamarre and Melville[16,17] measured the void fraction in the bubble plumes beneath six of the 2-D and 3-D breaking events. The eigenfrequencies were calculated by using these void-fraction measurements to obtain the sound speed within the plumes and the radii of the plumes. The estimated eigenfrequencies were found to closely match the observed spectral peaks indicating that the bubble plumes were oscillating collectively in the volume mode.

I. EXPERIMENTAL PROCEDURE: 2-D BREAKING

The 2-D experiments were conducted in a steel-framed glass-walled wave channel 25 m long, 0.76 m wide filled with 0.6 m of fresh water. A schematic of the experimental equipment and the wave channel is shown in Fig. 1. Breaking waves were generated by focusing a dispersive wave packet at a point x_b down the channel. The wave packets were synthesized from N sinusoidal components of constant slope ak, where a is the component amplitude and k is the component wave number. The components were equally spaced over a frequency bandwidth Δf, centered at frequency f_c. This method of generating breaking waves has been used previously to study the energy dissipation and wave forces produced by deep-water breaking waves.[18,19] In the present experiments, $\Delta f/f_c$, $x_b k_c$, and N were held constant at 1.0, 24.6, and 32, respectively, and S, the slope parameter defined as $S=Nak$, was varied. Over the range of slopes used in these experiments the breaking events were single spilling or plunging breakers. The waves generated are 2D, that is, there is negligible variation of the wave profile in the transverse direction across the channel prior to breaking. Table I lists the characteristics of the three wave packets used in the 2-D breaking experiments.

Underwater sound measurements were made with a set of calibrated omnidirectional International Transducer Corporation model ITC 1089E spherical hydrophones. The frequency response of the hydrophones is flat to within ± 1 dB from 10 Hz to 35 kHz and a typical sensitivity is -212 dB *re*: 1 V/μPa. The signals were amplified with Wilcoxon model AM-5 amplifiers set at 60-dB gain then bandpass filtered from 20 Hz to 10 kHz with Frequency Devices digitally programmable, four-pole Butterworth, model 874P8B-3 high-pass filters, and model 844P8B-5 low-pass filters, and then sampled digitally at 20 kHz. The hydrophones were located in the center of the channel at a depth of 37 cm from the free surface.

Measurements of the sound in air were made using a Shure SM81 cardioid condenser microphone. The microphone's frequency response is flat (± 1 dB typically) from 20 Hz to 20 kHz. The microphone was mounted vertically pointing downward 50 cm above the still water surface

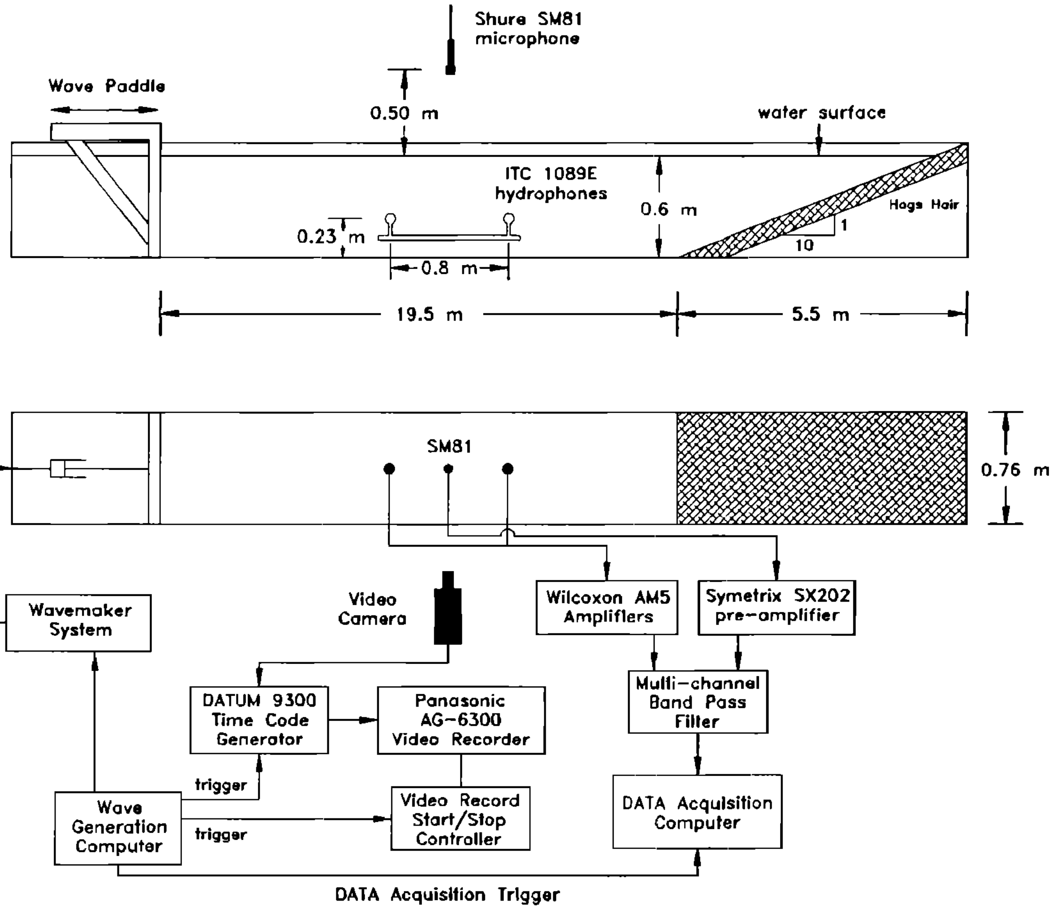

FIG. 1. Schematic drawing of an elevation view (top) and plan view (bottom) of the 25 m×0.76 m×0.60 m wave channel at MIT. The configuration of the experimental equipment is also illustrated.

directly above the most energetic part of the breaking event. The microphone signal was filtered and sampled in the same manner as the hydrophone signals.

II. RESULTS: 2-D BREAKING

The surface displacement was measured with resistance wire wave gauges in another series of experiments in which the void fraction was measured for the same wave packets.[16] The calibration procedure and measurement technique are described in detail in Loewen and Melville.[20]

It has been shown that the surface displacement variance can be used to estimate the momentum flux of weakly nonlinear, slowly varying, 2-D, deep water waves.[19] The surface displacement variance $\overline{\eta^2}$ is given by,

$$\overline{\eta^2}=\frac{1}{T}\int_0^T \eta^2(t)\,dt, \tag{2}$$

TABLE I. Wave packet characteristics; $\Delta f/f_c=1.0$ and $x_b k_c=24.6$ for all wave packets.

Wave packet	W_1	W_2	W_3
Center frequency, f_c (Hz)	0.78	0.88	0.98
Theoretical break point, x_b (m)	9.25	7.58	6.25
Center component wave number k_c (m^{-1})	2.66	3.25	3.93
Center component phase speed, c_c (m/s)	1.84	1.70	1.57

where $\eta(t)$ is the surface displacement and T is the length of the sampling interval. The fractional energy dissipation D due to breaking, is given by

$$D=(\overline{\eta_0^2}-\overline{\eta_f^2})/\overline{\eta_0^2}, \tag{3}$$

where $\overline{\eta_0^2}$ and $\overline{\eta_f^2}$ are the surface displacement variances upstream and downstream of the event.

The glass wave channel acts as a waveguide for underwater sound propagation. The free surface acts as a pressure release boundary and the glass sidewalls and bottom are surfaces with finite impedances. We can estimate the cutoff frequency of the lowest propagating mode by calculating the values for the two limiting cases. If we assume the glass has an infinite impedance, the cutoff frequency of the lowest mode is approximately 1200 Hz. If we assume the glass has an impedance of zero, the cutoff frequency of the lowest mode equals 1600 Hz. Therefore we expect the actual cutoff frequency of the lowest propagating mode to be between 1200 and 1600 Hz. The three hydrophones were spaced evenly over an 80-cm interval directly beneath the breaking events to avoid cutting off the signals below the lowest cutoff frequency. The microphone was placed directly above the breaking events to maximize the signal-to-noise ratio. A typical hydrophone time series and the corresponding spectrographs, for packet W_2 with $S=0.544$, are shown in Fig. 2.

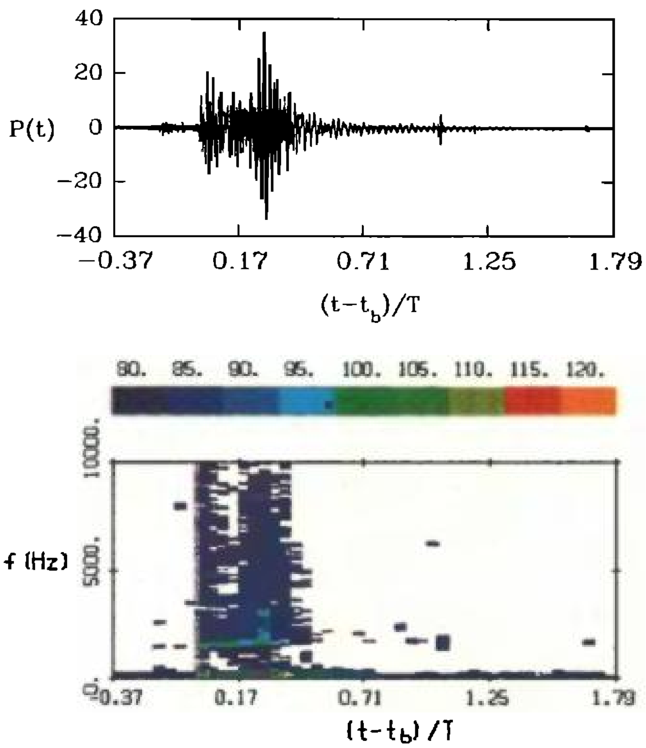

FIG. 2. The upper plot is a time series of the upstream hydrophone signal bandpass filtered from 20 Hz to 10 kHz for the 2-D packet W_2 with $S=0.544$. The lower plot is a spectrograph of the time series in the upper plot. Each color corresponds to a 5 dB *re*: 1 μPa^2 increment in the pressure spectrum level.

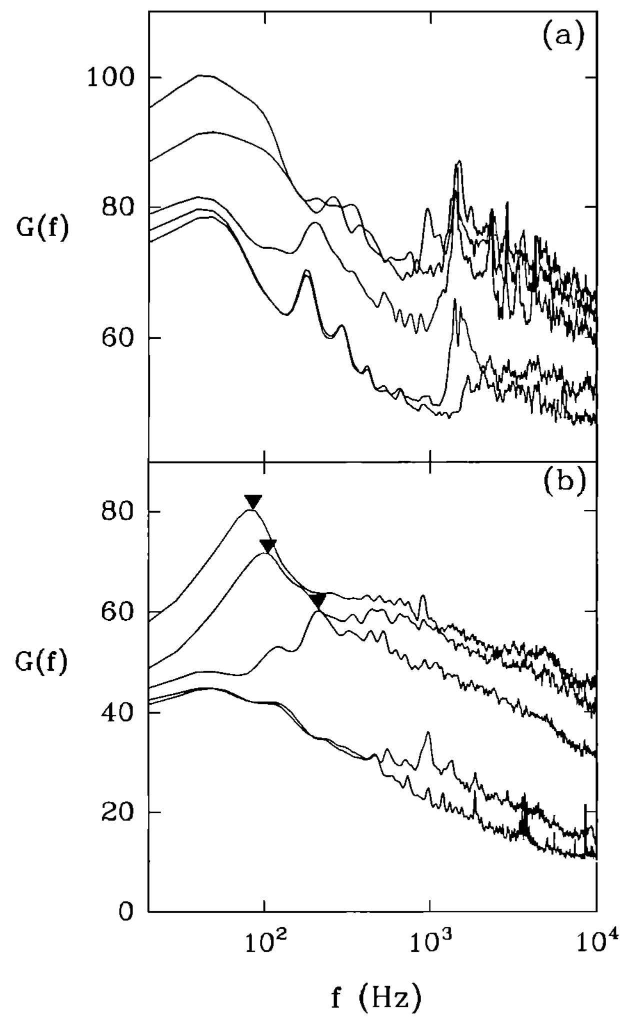

FIG. 3. Pressure spectrum level, $G(f)$ in dB *re*: 1 $\mu Pa^2/Hz$ of (a) hydrophone and (b) microphone signals for the 2-D packet W_1 with slope, $S=0.288$, 0.320, 0.352, 0.416, and 0.512. Each spectrum is the average of five repeats and has 80 deg of freedom. The ▼ symbols mark the locations of the spectral peaks associated with bubble plume oscillations.

In Fig. 3(a) and (b) averaged frequency spectra of the hydrophone and microphone signals, for packet W_1 over the range of wave slopes from 0.288 to 0.512 are shown. At the lowest slope of 0.288 no breaking occurs, however if the slope is increased slightly, breaking will occur. This wave is referred to as the incipient breaking wave. The spectrum for the incipient case is the lowest spectrum in each plot and can be considered the background noise level. The sharp peaks in the hydrophone spectra in Fig. 3(a) at frequencies greater than 1500 Hz are associated with the various cutoff frequencies of the propagating acoustic modes. The lowest cutoff frequency observed is at 1500 Hz which is between the limits predicted earlier.

The microphone signals were not directly influenced by the properties of the wave channel and therefore the microphone spectra plotted in Fig. 3(b) do not exhibit features consistent with a modal structure. The spectra slope at -4 to -6 dB per octave from 500 Hz to 10 kHz and there are large-amplitude low-frequency peaks in the microphone spectra of the larger slope breaking events which are marked with the symbol ▼ in Fig. 3(b). We will show in Sec. VI that these low-frequency signals are consistent with the collective oscillation of the entrained bubble plumes. The hydrophone spectra have much broader low-frequency peaks and this additional low-frequency energy may be caused by structural vibrations of the wave channel in response to the more energetic breaking events. This additional energy at low frequencies makes it impossible to detect the spectral peaks caused by the collective oscillations of the plumes in the hydrophone spectra in Fig. 3(a). However, we will show in Sec. VI that it is possible to detect these peaks in the hydrophone data using joint time-frequency analysis.

Both the hydrophone and microphone spectra clearly show that significant increases in spectral levels were produced by the breaking waves across the entire spectrum from 20 Hz to 10 kHz. Although some of the lower frequency energy in the hydrophone spectra may be due to vibrations of the tank, it is clear from the microphone spectra that there is significant low-frequency energy present which is not associated with tank response. At frequencies greater than 500 Hz there was a consistent increase in spectral levels as the wave slope was increased from the incipient value to the maximum value. However, at frequencies below 500 Hz there was no change in spectral levels when the slope was increased from the incipient value of 0.288 to 0.320. When the slope was increased further to 0.352, the spectral levels below 500 Hz increased dramatically. Video recordings showed that at a slope of 0.320, the event was a spilling breaker and at a slope of

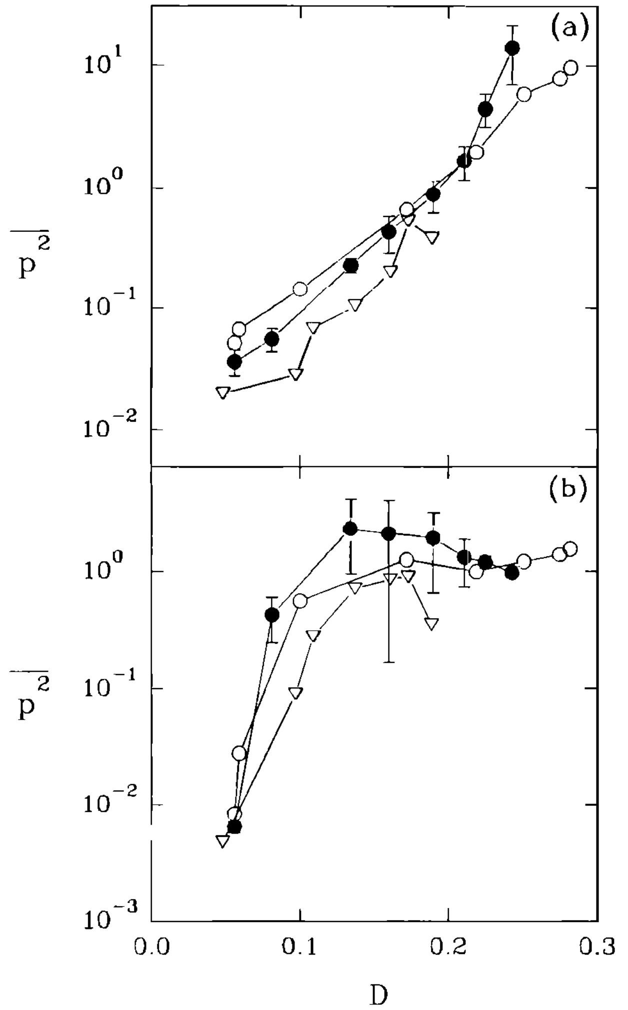

FIG. 4. The mean-square pressure $\overline{p^2}$ (Pa^2) of the hydrophone signal in two frequency bands (a) 20 Hz to 1 kHz and (b) 1 kHz to 10 kHz as a function of the fractional dissipation D. Each data point is the average of five repeats of the measurement and the error bars indicate the 95% confidence limits. ○, W_1; ●, W_2; ▽, W_3.

0.352, it was a plunging breaker. These data indicate that spilling waves do not generate significant low-frequency pressure signals and that the transition from spilling to plunging breaking may be clearly evident in the measured spectra. Similar results were observed in the sound spectra for the other two wave packets W_2 and W_3.

The mean-square pressures measured by the hydrophone in the two frequency bands from 20 Hz to 1 kHz and from 1 to 10 kHz are plotted versus the fractional dissipation in Fig. 4. The log of the mean-square pressure of the hydrophone signal in the lower-frequency band plotted in Fig. 4(a) correlates closely with the fractional dissipation. The log of the mean-square pressure in the higher-frequency band, shown in Fig. 4(b), increases rapidly with dissipation in the range $D=0.05$ to 0.14. For larger values of D the data reach a maximum value and then remain constant or decrease slightly. There is no consistent dependence on the wavelength of the packet evident in either the low- or high-frequency mean-square pressure data. There is less variability in the low-frequency data compared to the high-frequency data.

III. EXPERIMENTAL PROCEDURE: 3D BREAKING

The 3-D breaking experiments were conducted in a wave basin 45.7 m long by 30.5 m wide filled with 5.8 m of fresh water at the Offshore Technology Research Center (OTRC) at Texas A&M University. Measurements were made of the sound produced by breaking waves. Plan and elevation views of this facility are shown in Fig. 5. The channel was equipped with 48 independently controlled hinged wave paddles along the 30.5-m-wide endwall. The paddles were hinged at a point 3 m below the still water level. The waves were absorbed at the opposite end of the tank by a series of metal screens installed vertically extending from the tank bottom to several meters above the still water level. The tank was equipped with a motorized instrument platform which spanned the width of the tank and could be accurately positioned to within ±0.25 cm.

Three-dimensional breaking waves were produced by focusing wave components radially (a so-called "bulls eye" pattern) to a point along the centerline of the channel and focusing the different frequency components in a similar manner to the scheme described for the 2-D breaking experiments in Sec. I. The amplitude of the waves was varied by adjusting the gain of the signal sent to the wave paddles. The wave amplitude is a maximum at the center of the tank and decreases toward the sidewalls. This technique produces circular wave crests which curve concavely toward an observer stationed downstream of the wave paddles and the wave field is symmetric about the longitudinal centerline.

The surface displacement was measured with a series of capacitance wire wave gauges. The surface displacement data were sampled at a rate of 200 Hz. Five wave gauges spaced at 2.4-m intervals were mounted from the instrument platform, the position of each gauge is shown in Fig. 5. Measurements of the surface displacement were made at 10-ft (3-m) intervals along the length of the basin. The gauges consisted of Teflon coated wire mounted on $\frac{1}{4}$-in. stainless-steel frames. The gauges were calibrated by sampling the still water level in 7.5-in. (19-cm) increments over a 30-in. (76-cm) range. The relationship between the wave amplitude and the output voltage was linear and the gauges were calibrated once a day. The linear term in the calibration equation varied by approximately ±2% from one day to the next.

Underwater video recordings were made of some of the experimental runs. The video equipment used was the same as that described in Sec. I. Underwater sound measurements were made with two omnidirectional B&K model 8105 hydrophones and two B&K model 2635 charge amplifiers. The acoustic data were bandpassed filtered in the range 10 Hz to 20 kHz (using the same filters as described in Sec. I) and sampled digitally at 40 kHz per channel.

In both the 2-D and 3-D experiments we took great care to place the hydrophones a short distance outside the turbulent two-phase flow formed by the breaking waves. In the 3-D experiments the hydrophones were located 1.9 m below the still water level and the largest diameter of plume observed was approximately 60 cm. Therefore, the

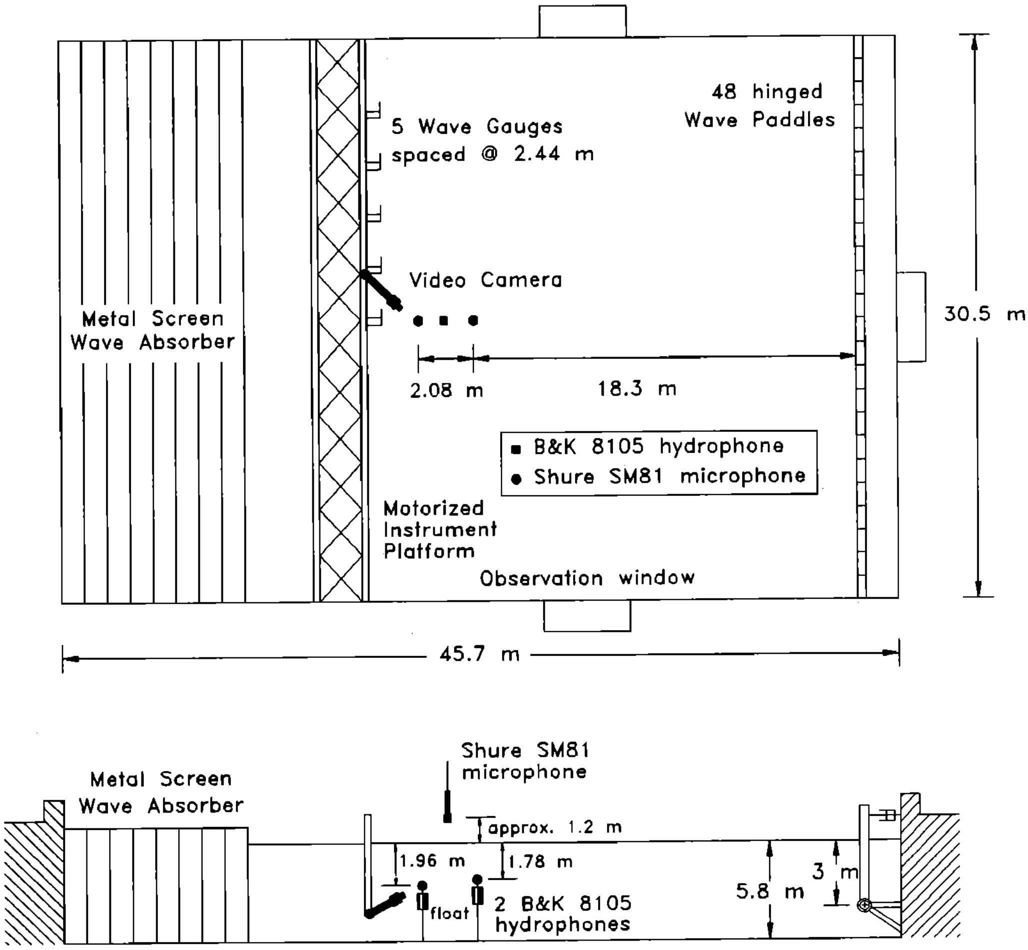

FIG. 5. A drawing of a plan (top plot) and elevation view (bottom plot) of the three-dimensional wave channel at the Offshore Technology Research Center at Texas A&M University. The layout of some of the experimental equipment is also shown.

hydrophones were located a minimum of 1.3-m below the bottom edge of the entrained plume well away from the turbulent flow. In the 2-D experiments three hydrophones were positioned along an 80-cm interval, 37-cm below the free surface beneath the breaking events. The data presented here were sampled with the hydrophone located closest to the wave paddle, slightly upstream of the breaking events. The largest diameter plume observed in the 2-D experiments had a diameter of approximately 30 cm and therefore the sampling hydrophone was located a minimum of 50 cm from the edge of the plume. As a result we are confident that none of the measurements were significantly influenced by noise generated by turbulent flow past the transducers.

IV. RESULTS: 3-D BREAKING

The hydrophones were mounted approximately 1.9 m below the water surface 3.9-m above the tank bottom directly below the breaking waves. They were placed close to the breaking events to improve the signal-to-noise ratio. The sparseness of the wave gauge array and the lack of complete wave absorption in the basin prevented measurements of the energy loss from the wave field due to breaking. As a result we used the gain of the signal G, sent to the wave paddles as a measure of the amplitude of the 3-D breaking waves.

Figure 6 shows a typical time series and spectrograph of a signal received by a hydrophone. These data are for the largest amplitude wave with gain, $G=0.70$. The signal was bandpass filtered from 10 Hz to 20 kHz and notch filtered from 200 to 340 Hz to reduce the strength of the noise from the wave maker hydraulic system in this frequency range. The underwater sound, due to breaking, is almost hidden in the background noise in the time series in Fig. 6. However, it is easily detected in the spectrograph where the spectral levels over the entire frequency range from 10 Hz to 20 kHz increase 10 to 20 dB above the background noise levels at $t_*=(t-t_b)/T=0.0$, where t is the time referenced to the start of the wave paddle motion, t_b is the time when breaking begins, and T is the period of the wave packet center component. The wave plunges and impacts the free surface at $t_*=0.0$.

Frequency spectra averaged over five repeats of the same breaking events are shown plotted in Fig. 7 for one channel of hydrophone data. The four spectra correspond to G in the range 0.24 to 0.70. The lowest gain, $G=0.24$, is the incipient case for which no breaking occurs and in Fig. 7 it is the lowest amplitude spectra. The frequency band

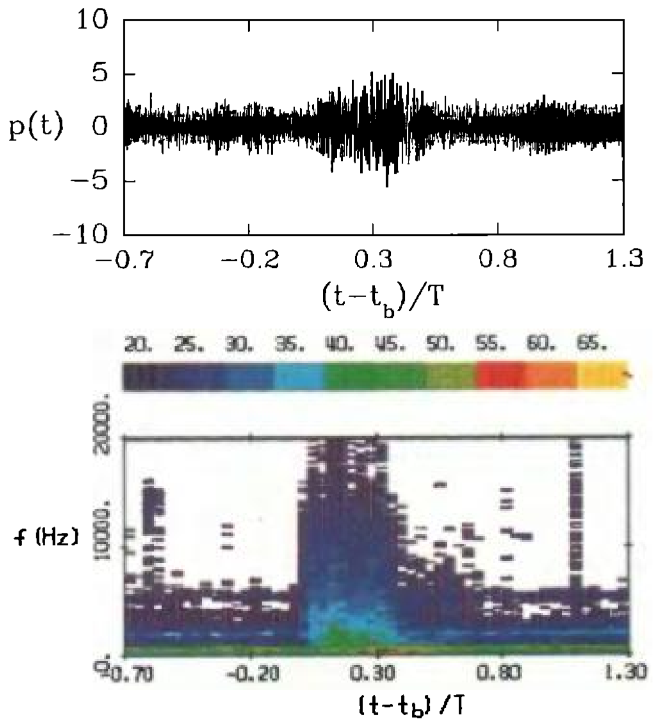

FIG. 6. The upper plot is a time series of the signal from the downstream hydrophone bandpass filtered from 10 Hz to 20 kHz and band reject filtered from 200 to 340 Hz for the 3-D event with gain, G=0.70. The lower plot is a spectrograph of the time series in the upper plot. Each color corresponds to a 5 dB *re*: 1 μPa^2 increment in pressure spectrum level.

from 150 Hz to 1 kHz in the underwater sound data is dominated by background machinery generated noise. Noise from the wave maker hydraulic system produced the large amplitude spectral peaks at 190, 280, and 520 Hz. The hydrophone spectra show almost no variation in spec-

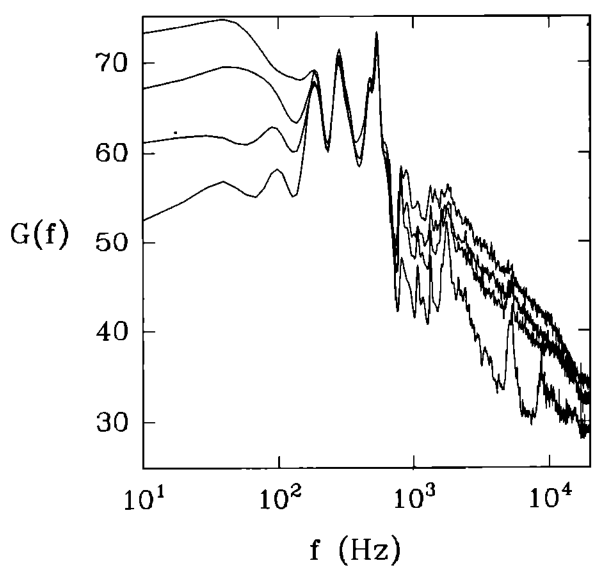

FIG. 7. Pressure spectrum level $G(f)$ in dB *re*: 1 $\mu Pa^2/Hz$ of the signal from the downstream hydrophone bandpass filtered from 10 Hz to 20 kHz and band reject filtered from 200 to 340 Hz for the 3-D events with gains, G=0.24, 0.40, 0.55, and 0.70. Each spectrum was averaged over five repeats of the same event and has 80 deg of freedom.

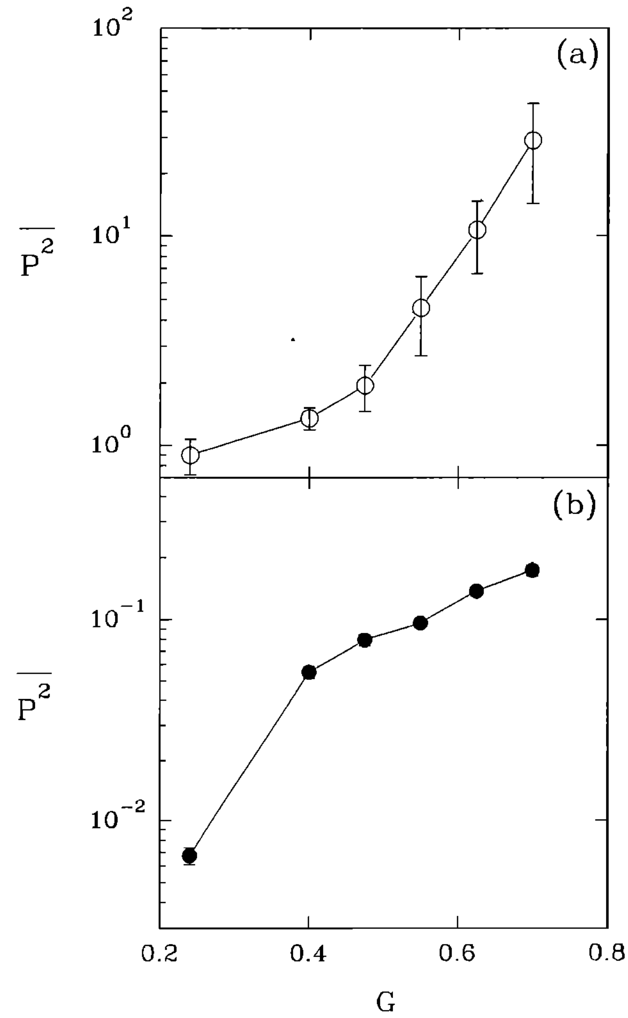

FIG. 8. Mean-square pressure $\overline{p^2}$ (Pa^2) of the downstream hydrophone signal in two frequency bands (a) 10 to 150 Hz and (b) 1 to 20 kHz as a function of the gain G. Each data point is the average of at least three repeats of the same event and the error bars indicate the 95% confidence limits of the data.

tral levels with increasing wave amplitude in the frequency range from 150 Hz to 1 kHz, indicative of a very poor signal-to-noise ratio.

The hydrophone spectra have several notable features. The lowest amplitude event for which breaking occurred had a gain, G=0.40, and the spectral levels for this event are 5 to 10 dB higher than those for the incipient event. There is significant low-frequency energy in the spectra at frequencies less than 200 Hz and this energy increased as the amplitude of the breaking event was increased. For frequencies greater than 1 kHz the underwater sound spectra have an almost constant slope of −5 to −6 dB per octave and the levels increased consistently as the amplitude of the waves was increased.

To avoid the noise generated by the wave maker hydraulic system the mean-square pressure was calculated in the frequency bands from 10 Hz to 150 Hz and from 1 kHz to 20 kHz. The mean-square pressure, $\overline{p^2}$, in these two frequency bands was calculated over the entire signal duration for the hydrophone data and is shown plotted as a function of the gain in Fig. 8(a) and (b), respectively. In

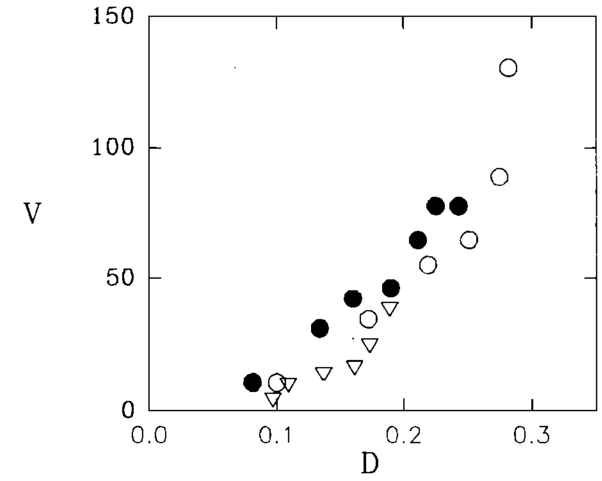

FIG. 9. The volume per unit width V (cm^2) of air in the cylinder formed by the plunging wave crest versus the fractional dissipation D for the three wave packets in the 2-D breaking experiments. ○, W_1; ●, W_2; ▽, W_3.

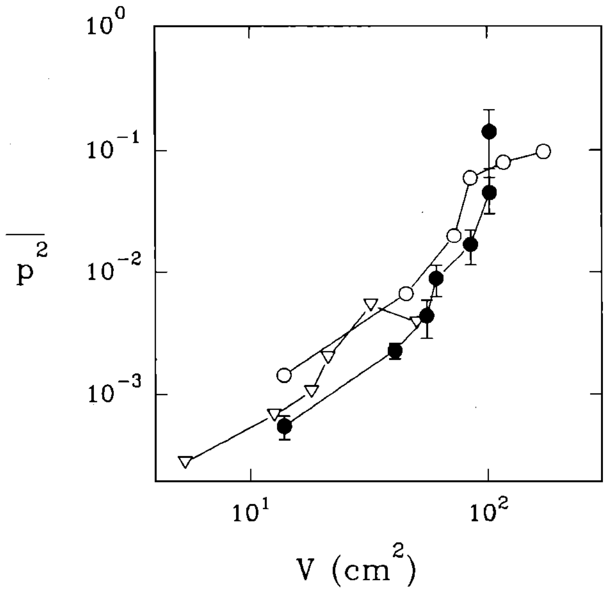

FIG. 10. The mean-square pressure $\overline{p^2}$ (Pa^2) of the signal from the upstream hydrophone in the frequency band from 20 Hz to 1 kHz as a function of the volume per unit width of the cylinder V (cm^2). Each data point is the average of five repeats of the measurement and the error bars indicate the 95% confidence limits. ○, W_1; ●, W_2; ▽, W_3.

the higher-frequency band there is strong correlation between the log of the mean-square pressure and the wave amplitude. The mean-square pressure in the lower-frequency band also correlates well with the gain however the scatter in the data is slightly greater than for the data in the higher-frequency band.

V. VOLUME OF ENTRAINED AIR

Lamarre and Melville[16] have shown that the process of air entrainment by 2-D plunging breakers scales with the prebreaking wave variables and that the bulk properties of the bubble plume evolve according to simple functions of time. They found that the volume of entrained air decreases exponentially with time from a maximum value corresponding to the volume initially enclosed by the plunging wave crest. From video recordings of the 2-D breaking events it was possible to measure the size of the cylinder of air initially enclosed by the plunging breakers. This was possible for all but the lowest one or two amplitude breakers for each of the three wave packets. From the cylinder size the volume of air initially enclosed was calculated.

In Fig. 9 the fractional dissipation is plotted versus the volume of air per unit width. There is a strong correlation and the volume of air per unit width increases linearly as the dissipation increases. The strong correlation indicates that the amount of energy dissipated by breaking and the volume of air entrained are closely related. This relationship was first observed by Lamarre and Melville[16] who found that up to 50% of the energy dissipated by breaking was expended entraining air against the buoyancy force. They measured the void faction beneath wave packet W_2 for three breaking events with slopes, $S=0.544$, 0.448, and 0.384. They observed that the ratio of the energy dissipated by breaking to the volume of air entrained remained constant and from this they concluded that the initial volume of air entrained would correlate with the energy dissipation. This hypothesis is confirmed by the data in Fig. 9.

The mean-square pressure in the frequency band from 20 Hz to 1 kHz, for the 2-D breaking events is plotted as a function of the volume of air per unit width in Fig. 10. There is a strong correlation between the mean-square pressure in the frequency band from 20 Hz to 1 kHz and the volume of air entrained. The data for the highest-frequency wave packet W_3, do not correlate as well with the volume of air as the data for the lower two frequency packets, and this was also the case for the correlation versus dissipation (see Fig. 4).

VI. COLLECTIVE BUBBLE PLUME OSCILLATIONS

In Fig. 11 spectrographs of the microphone and hydrophone signals averaged over five repeats of a 2-D breaking event are shown. There is a low-frequency signal which begins at $t_*=0.0$ and another slightly lower-frequency signal which begins at $t_*=0.20$. The origin of the low-frequency signals, which occurred immediately following the impact of the plunging crest ($t_*=0.0$) in the 2-D breaking experiments, has been investigated thoroughly and those results will be presented in another paper. For the purposes of this work it is sufficient to state that we have concluded that these low-frequency signals are produced by the volumetric pulsation of the cylinder of pure air (100% void fraction) entrapped by the plunging wave crest. The beginning of the second low-frequency signal, at $t_*=0.20$, coincides with the time at which the cylinder of pure air breaks up to form a bubble plume. These low-frequency spectral peaks were not detectable in the time-averaged hydrophone spectra (see Fig. 3). However, as can be seen in Fig. 11, they are easily detected in the color spectrographs.

Low-frequency spectral peaks were also observed in the 3D breaking experiments. There were high levels of

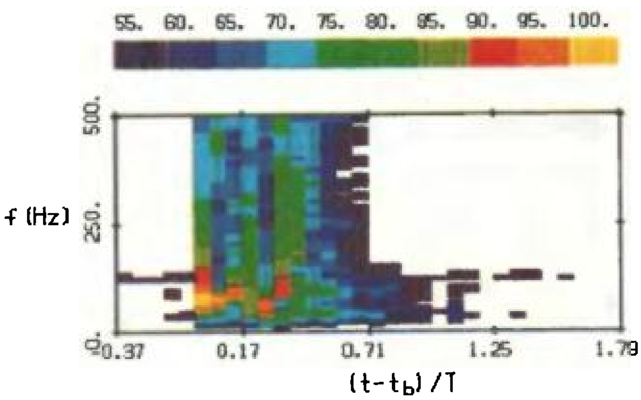

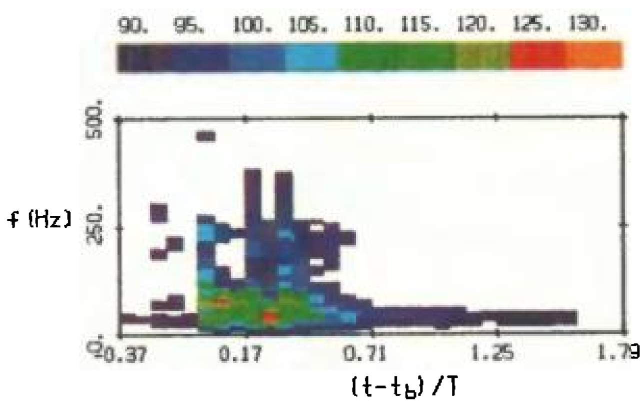

FIG. 11. Spectrographs of signals from the microphone (top) and the upstream hydrophone (bottom) for the 2-D packet W_2 with $S=0.544$. The spectra were averaged over five repeats of the event and each color corresponds to a 5 dB *re*: 1 μPa^2 increment in pressure spectrum level.

background noise present in the 3-D experiments and in order to detect the spectral peaks associated with the bubble plumes it was necessary to subtract the background noise spectrum from the spectra displayed in the color spectrographs. Figure 12 shows a spectrograph averaged from five repeats of the largest 3-D breaking wave where the background noise spectrum has been subtracted from the data. After this processing the low-frequency peaks are

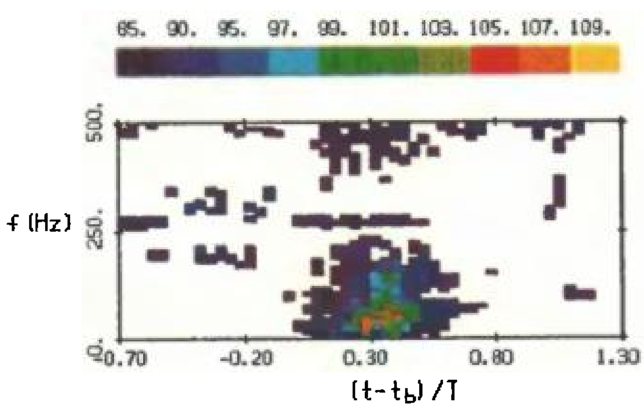

FIG. 12. Spectrograph of a signal from the downstream hydrophone for the 3-D packet with $G=0.70$. The spectra were averaged over five repeats of the event and each color corresponds to a 2 or 5 dB *re*: 1 μPa^2 increment in pressure spectrum level. The background noise spectrum was subtracted from the data.

clearly visible in the spectrographs. In Fig. 12 higher-frequency sound generation begins at $t_*=0.0$ (also see Fig. 6) and large low-frequency spectral peaks appear at approximately $t_*=0.30$. It was our hypothesis that these low-frequency signals which begin $\frac{1}{5}$ to $\frac{1}{3}$ of a wave period after the start of breaking beneath the 2-D and 3-D breaking waves were caused by the collective oscillation of the bubble plumes.

Theoretical predictions of the resonant frequencies or eigenfrequencies of bubble plumes have been made previously by Lu *et al.*[15] and Carey *et al.*[12] Eigenfrequencies were predicted by Lu *et al.*[15] based on the assumption that the bubble plumes were freely oscillating. Carey *et al.*[12] derived an expression for the lowest eigenfrequency of a spherical bubble plume by assuming the oscillations were forced by an external source of excitation. We followed an approach similar to that of Lu *et al.*[15] in order to calculate the eigenfrequencies of the observed bubble plumes.

First we consider a cylindrical bubble plume of finite length which oscillates harmonically with time. We assumed that the plume is comprised of small air bubbles whose resonant frequencies are much greater than the resonant frequencies of the entire plume. The air–water mixture within the plume is taken to be a continuum and only linear oscillations are considered.[15] The sound speed inside the plume, $r<R_c$, is constant and equal to c_m and outside the plume in the pure liquid, $r>R_c$, the sound speed is constant and equal to c. Therefore the sound pressure inside and outside of the plume must satisfy the homogeneous Helmholtz equation,

$$\nabla^2 P+k^2 P=0, \tag{4}$$

where P is the pressure and k is the wave number equal to k_m inside the plume and k_0 outside. The boundary conditions applied at the plume edge at $r=R_c$ are that the pressure and the normal velocity or the gradient of the pressure are continuous,

$$P^0=P, \quad \frac{\partial P^0}{\partial r}=\frac{\partial P}{\partial r}, \tag{5}$$

where P^0 equals the pressure outside the plume and P is the pressure inside the plume. The radiation boundary condition is applied as the radius goes to infinity and the condition that the solution remain finite inside the plume is also enforced. We have assumed the plume is immersed in an infinitely large tank and we discuss the implications of this assumption in Sec. VII. The solution to the Helmholtz equation for each mode inside the plume is given by

$$P=A_n J_n(r\sqrt{k_m^2-\kappa^2})e^{i\kappa z}e^{in\theta}e^{i\omega t}, \tag{6}$$

where P is the pressure, A_n is an amplitude coefficient, n is the mode number, J_n is a Bessel function of the first kind, κ is the wave number in the z direction (the z axis is along the axis of the cylinder), and θ is the azimuthal angle. The solution to the Helmholtz equation outside the plume in the pure liquid is given by

$$P^0=B_n H_n^{(2)}(r\sqrt{k_0^2-\kappa^2})e^{i\kappa z}e^{in\theta}e^{i\omega t}, \tag{7}$$

where P^0 is the pressure outside the plume, B_n is an amplitude coefficient, $H_n^{(2)}$ is a Hankel function of the second kind, and k_0 is the wave number in the pure liquid. The variation of the pressure in the z direction along the axis of the cylinder is specified by setting κ equal to a constant. If $\kappa=\pi/w$, where w is the plume length, this sets the wavelength in the z direction equal to twice the plume length and this corresponds to a plume with pressure release or rigid boundary conditions at its ends. If we set $\kappa=0$ the wavelength in the z direction is infinite and this corresponds to a 2-D cylinder of infinite length.

At the edge of the plume at $r=R_c$ the boundary conditions given in Eq. (5) are imposed and the following characteristic equation is derived

$$s\frac{H_{n-1}^{(2)}(s)}{H_n^{(2)}(s)}-x\frac{J_{n-1}(x)}{J_n(x)}=0, \tag{8}$$

where $x = R_c\sqrt{k_m^2-\kappa^2}$ and $s = R_c\sqrt{k_0^2-\kappa^2}$. The roots of this characteristic equation for a given mode number n correspond to the eigenfrequencies of the cylindrical bubble plume for that mode.

To solve for the roots of Eq. (8) we need to know k_0, k_m, and κ. The frequency is assumed to be complex and is given by

$$\omega=2\pi f_R+if_I. \tag{9}$$

If we assume the bubbles within the plume are all of equal radius a, the wave number inside the bubble plume in the air–water mixture is given by the following dispersion relation:

$$k_m^2=\frac{\omega^2}{c^2}+4\pi\omega^2\frac{Na}{\omega_0^2-\omega^2+2ib\omega}, \tag{10}$$

where N is the number of bubbles per unit volume, c is the speed of sound in the pure liquid, and

$$\omega_0^2=\frac{P_0}{\rho a^2}\,\mathrm{Re}(\Phi), \tag{11}$$

$$b=\frac{2\mu}{\rho a^2}+\frac{P_0}{2\rho(2\pi f_R)a^2}\,\mathrm{Im}(\Phi)+\frac{(2\pi f_R)^2a}{2c}, \tag{12}$$

where ω_0 is the resonant frequency of a bubble with radius a, b is the damping constant of a single bubble with radius a, μ is the viscosity of pure water, ρ is the density of pure water, P_0 is the equilibrium pressure inside the bubble, and Φ is given by

$$\Phi=\frac{3\gamma}{1-3(\gamma-1)i\chi[(i/\chi)^{1/2}\coth(i/\chi)^{1/2}-1]}, \tag{13}$$

where γ is the ratio of the specific heats and χ is given by

$$\chi=D/\omega a^2, \tag{14}$$

where D is the thermal diffusivity of air.[15,21,22] The wave number in the mixture k_m is complex and the wave number in the pure liquid k_0 is real and given by $k_0=(2\pi f_R)/c$. Therefore, the acoustic pressure both inside and outside of the plume decays exponentially with time because ω is complex. Inside the plume the acoustic pressure decays exponentially as it propagates in the r direction because k_m is complex. Outside the plume there is no exponential decay associated with the propagation of the sound in the radial direction. The damping of the sound is due to the presence of the air bubbles inside the plume and the damping constant associated with a single bubble given by Eq. (12) is included explicitly in the expression for k_m, Eq. (10).

This formulation includes the assumption that the bubbles do not interact directly with the pressure fields of adjacent bubbles but only with the average field.[21] As a result, it is thought that this theory is only valid for sound propagation in bubbly mixtures with void fraction below a few percent. However Commander and Prosperetti[21] predicted the attenuation coefficient in a bubbly mixture with a void fraction of 10% and obtained reasonable agreement with the observed values of Ruggles *et al.*[23] This suggests that the theory may be used with some confidence at higher void fractions as well. The reader is referred to Refs. 15, 21, and 22 for more details on the propagation of sound in bubbly liquids and the derivations of Eqs. (10)–(13).

Based on the void fraction measurements of Lamarre and Melville,[16,17] we concluded that the most accurate simple geometric model of the observed plumes was a semicircular cylindrical plume located immediately below the free surface. This is demonstrated very clearly in Fig. 9 of Lamarre and Melville[17] which shows a contour map of the void-fraction field for a 3-D breaking event plotted together with the equivalent semicircular model plume. It is evident from a comparison of these two figures that a semicircular plume located immediately below the free surface is a good geometric model of the observed plumes.

We can compute the resonant frequencies of a semicircular plume located below the free surface using the solution developed for the circular plume in Eqs. (4) to (14). The additional constraint we must impose in order to satisfy the pressure release boundary condition at the free surface is that the mode number n must be odd. This ensures that the pressures inside and outside the plume P and P^0, respectively, are equal to zero on the free surface or the plane defined by $\theta=\pi/2$ and $\theta=-\pi/2$, where θ is the azimuthal angle measured clockwise from the positive z axis, which points downward. That is, the solutions for P and P^0 given by Eqs. (6) and (7) both equal zero when n is odd and $\theta=\pi/2$ and $\theta=-\pi/2$. Therefore when n is odd, the solution defined by Eqs. (4) to (7) satisfies the Helmholtz equation inside and outside of the plume and it also satisfies the boundary conditions at the plume edge at $r=R_c$ and at the free surface. This is the same approach that Lu *et al.*[15] took when they modeled a bubble plume generated by a single breaking event as a hemispherical cloud at the free surface. Using this approach, the radius of the model plumes is given by

$$R_c=\sqrt{2A_{ob}/\pi}, \tag{15}$$

where R_c is the radius of the model plume and A_{ob} is the cross-sectional area of the observed plume. The lowest mode of the semicircular cylindrical plumes occurs when $n=1$. This is the volume or breathing mode because it corresponds to the case where the entire plume (half-cylinder) is volumetrically expanding and contracting in phase.

A semicircular cylindrical plume oscillating in its $n=1$ mode immediately below the free surface behaves as a dipole source. The total pressure field outside the plume, given by Eq. (7), is the sum of the pressure produced by the submerged half-cylinder as it oscillates volumetrically plus the pressure produced by its mirror image above the free surface (the two half-cylinders form a full cylinder with its axis on the free surface) which is also oscillating volumetrically but 180° out of phase with the submerged half-cylinder. In the far field, when $r\sqrt{k_0^2-\kappa^2} \gg 1$, Eq. (7) can be simplified using the asymptotic expression for $H_1^{(2)}$ to show that the pressure varies as $1/\sqrt{r}$ and the directional pattern of the pressure is given by $\cos(\theta)$. This is exactly the same far-field behavior as would be produced by a dipole source such as a fully cylindrical plume oscillating volumetrically ($n=0$ mode) beneath a pressure release surface.

The resonant frequencies for the lowest mode, $n=1$, can be determined by solving for the roots of Eq. (8) in the complex ω plane. The variation of the acoustic pressure field in the z direction is specified by setting the value of κ. A value of $\kappa=0$ corresponds to an infinitely long or 2-D semicircular plume. As stated earlier if $\kappa=\pi/w$, where w is the plume length in the z direction, this corresponds to the case in which the boundary conditions at the plume ends are taken to be pressure release or rigid. In the 2-D experiments the bubble plumes were bounded at each end by glass walls and therefore setting $\kappa=\pi/w$, where w is the wave channel width appears reasonable. In the 3-D experiments the width of the bubble plumes were only a fraction of the wave tank width and specifying the z dependence of the acoustic pressure is more difficult. However we will show that for the 2-D and 3-D breaking events, setting κ equal to 0 or π/w has very little effect on the predicted resonant frequencies.

For a given complex frequency ω and mean bubble radius a, χ and Φ were evaluated using Eqs. (13) and (14). Then, the values of the damping constant b and the resonant frequency ω_0 were calculated using Eqs. (11) and (12) (note that the real part of $\omega=2\pi f_R$ is used in these equations). The complex wave number in the plume k_m was then calculated using Eq. (10) (note that complex ω is used in calculating k_m) and the wave number in the pure liquid k_0 was equal to $2\pi f_R/c$. The measured cross-sectional area was used to calculate the radius of the model plume, R_c. Finally, the characteristic equation [Eq. (8)] was evaluated over a grid of points in the complex ω plane and the roots were located. The roots were found by plotting contours of the magnitudes of the real and imaginary parts of the characteristic equation in the complex ω plane and locating the intersection points of the zero contours.

In order to calculate the resonant frequencies of the observed bubble plumes the mean-void fraction inside the plume, the cross-sectional area of the plume, and the mean radius of the individual bubbles must be known. Void fraction measurements were available for three 2-D breaking events for the wave packet W_2 and for three wave amplitudes of the 3-D events and therefore the mean-void fraction and the plume cross-sectional area were known as functions of time for these six events.[16,17]

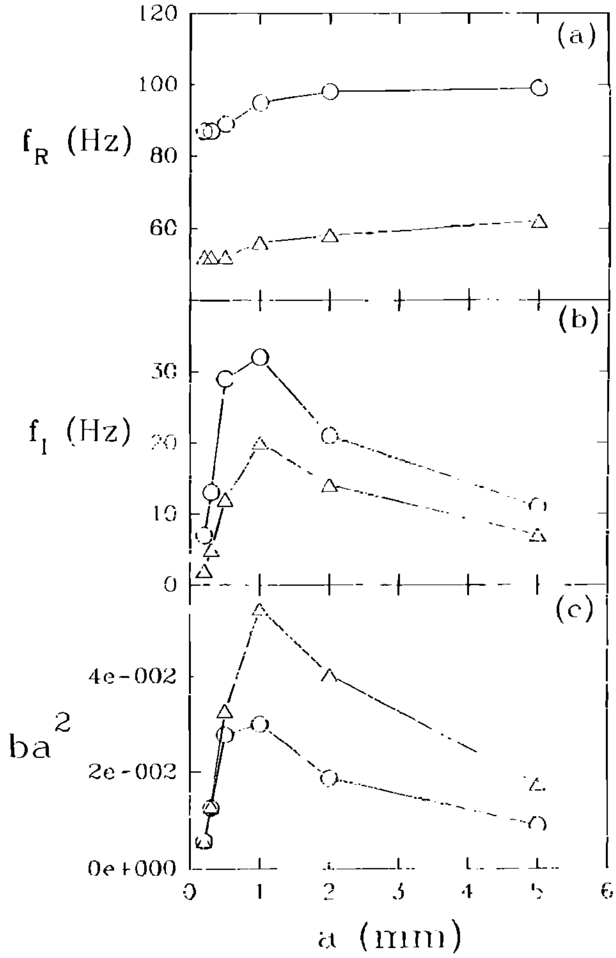

FIG. 13. (a) The predicted resonant frequency f_R and (b) damping rate f_I for two bubble plumes as a function of the bubble radius a. (c) The parameter ba^2 where b is the damping constant of a single bubble at the plume resonance frequency plotted as a function of the bubble radius a. O—R_c=0.256 m and $\bar{\alpha}$=0.030, Δ—R_c=0.162 m and $\bar{\alpha}$=0.207, where R_c is the radius of the plume.

Carey *et al.*[24] measured the bubble size distributions in fresh and salt water plumes produced by a tipping trough. They found that in both fresh and salt water the magnitude of the bubble size distributions peaked at 0.3 mm and fell sharply as the radius decreased. In fresh water they found that there was a secondary peak in the bubble size distribution which occurred at a radius of approximately 2.5 mm and there were very few bubbles larger than 5 mm. Based on these results we examined what effect varying the mean bubble radius over the range from 0.2 to 5 mm had on the theoretically predicted resonant frequencies.

Figure 13 shows a plot of the predicted resonant frequencies and the damping rates for two of the observed bubble plumes which have model plume radii of, R_c=0.162 and 0.256 m, and mean-void fractions, $\bar{\alpha}$=0.207 and 0.030, as a function of the mean bubble radius a. The plot shows that the predicted resonant frequencies are insensitive to large changes in the mean-bubble radius. As

TABLE II. Table of predicted bubble plume resonant frequency data. In column (1) the wave packet is identified, (2) the wave slope, S for 2-D events and the gain, G for 3-D events, (3) dimensionless time, (4) measured mean void fraction, (5) measured bubble plume cross-sectional area, (6) bubble plume resonant frequency for $\kappa=0$ or infinitely long plumes, (7) bubble plume resonant frequency for $\kappa=\pi/w$ (w=channel or plume width), and (8) $\kappa=\pi/w$ values. The resonant frequencies tabulated in columns (6) and (7) were obtained by solving for the complex roots of the characteristic equation given in Eq. (8).

1	2	3	4	5	6	7	8
Wave packet 2D—0.88 Hz or 3D	Wave slope or gain S or G	Dimensionless time $(t-t_b)/T$	Mean-void fraction $\bar{\alpha}$ (%)	Plume cross-sectional area A (cm^2)	Free oscillation resonant frequency [cf. Eq. (8)] f_R (Hz) (κ=0.0)	Free oscillation resonant frequency [cf. Eq. (8)] f_R (Hz) (κ as listed in column 8)	Transverse wave number $\kappa=\pi/w$
2D	0.540	0.16	20.67	411	56	61	4.13
2D	0.540	0.33	8.25	702	69	78	4.13
2D	0.540	0.51	2.95	1031	95	114	4.13
2D	0.448	0.32	10.08	371	86	93	4.13
2D	0.448	0.49	4.00	465	122	135	4.13
2D	0.448	0.67	2.05	432	179	198	4.13
2D	0.384	0.26	10.56	231	107	113	4.13
2D	0.384	0.44	3.77	351	147	159	4.13
2D	0.384	0.62	3.27	406	146	159	4.13
3D	0.70	0.10	21.25	1518	27	27	0.63
3D	0.70	0.25	8.37	2646	33	34	0.63
3D	0.70	0.35	3.51	2649	53	54	0.63
3D	0.55	0.23	10.00	1381	43	43	0.90
3D	0.55	0.38	2.63	2472	64	67	0.90
3D	0.55	0.48	2.05	2277	75	79	0.90
3D	0.40	0.20	6.70	1101	59	62	1.15
3D	0.40	0.30	3.19	1514	74	77	1.15
3D	0.40	0.40	2.12	1029	112	116	1.15

the bubble radius is increased from 0.2 to 5.0 mm, the predicted resonant frequencies increase by approximately 10%. The damping rate f_I is a maximum at a radius, $a=1$ mm, and decreases as the radius is increased or decreased. This result is unexpected because it is known that the damping constant b of a single bubble decreases monotonically as the radius is increased over this range of bubble radii.

Commander and Prosperetti[21] have shown that for a given mean-void fraction $\bar{\alpha}$, equilibrium bubble pressure P_0 and frequency ω if the resonant frequency of the individual bubbles ω_0 is much greater than ω, then the attenuation of a sound wave propagating through a bubbly mixture, given by the imaginary part of the wave number in the mixture, Imag(k_m), is proportional to (ba^2), the bubble radius squared, times the bubble damping constant. In Fig. 13(c) (ba^2), where b is the value of the bubble damping constant at resonance, is plotted as a function of the bubble radius. We note that the parameter (ba^2) has a maximum at $a=1$ mm and its dependence on the bubble radius is identical to that of the damping rate f_I. This indicates that the collective oscillations of bubble plumes comprised of 1-mm-radius bubbles will be more heavily damped than plumes containing either larger or smaller bubbles. These results also show that the eigenfrequency of the collective volume mode is not only insensitive to variations in the mean bubble radius but also to the damping rate. In fact, when the damping due to the presence of the air bubbles is neglected completely, that is, if the damping constant b is set equal to zero, the predicted eigenfrequencies increase by less than 3%.

The roots of the characteristic equation corresponding to the $n=1$ mode of a freely oscillating semicircular plume were evaluated for the six events for which void fraction data were available for $\kappa=0$ and $\kappa=\pi/w$. As we showed previously the predicted eigenfrequencies are insensitive to the mean bubble radius and therefore we assumed $a=1$ mm when computing the eigenfrequencies. These results are tabulated in Table II at three different times for each event. The results for $\kappa=0$ and $\kappa=\pi/w$ are in columns 6 and 7, respectively. Increasing κ from 0 to π/w caused the predicted resonant frequencies to increase by 5% to 10%. The effect is relatively small because in both the 2-D and 3-D experiments the ratio of the plume or channel width to the plume radii was 12 or greater.

We have shown that the eigenfrequencies of the volume mode can be accurately predicted when the plumes are assumed to be infinitely long, when the damping due to the presence of the air bubbles is neglected, and when the mean bubble radius is varied from 0.2 to 5 mm. In Fig. 14 we have plotted the resonant frequency f_R of the lowest mode ($n=1$) of a 2D ($\kappa=0$) semicircular cylindrical bubble plume located at the free surface as a function of the plume radius and mean-void fraction. In this figure we have taken the mean-bubble radius to be 1 mm. The four curves can be reduced to the following simple equation:

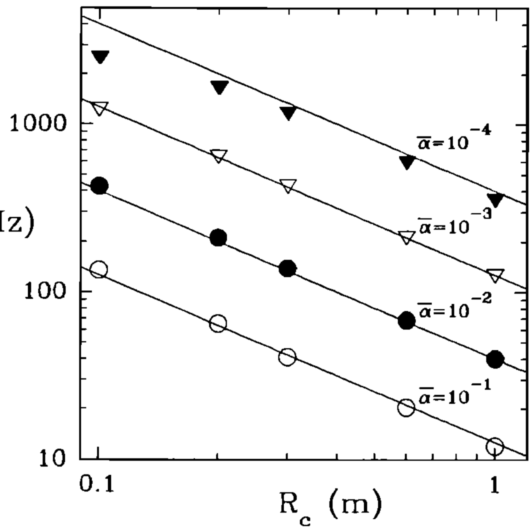

FIG. 14. The symbols are the predicted resonant frequencies f_R of the $n=1$ mode of a semicylindrical bubble plume of radius R_c located at the free surface. ○—$\bar{\alpha}=0.1$, ●—$\bar{\alpha}=0.01$, ▽—$\bar{\alpha}=0.001$, and ▼—$\bar{\alpha}=0.0001$. The solid curves are Eq. (16) evaluated at $\bar{\alpha}=0.1$, 0.01, 0.001, and 0.0001.

$$f_R=4.0/(R_c\sqrt{\bar{\alpha}})=c_m/(2.5R_c), \tag{16}$$

where we have used the low-frequency approximation for c_m given by

$$c_m=\sqrt{P_0/(\rho\bar{\alpha})}, \tag{17}$$

where we have taken $P_0=101$ kPa and $\rho=1000$ kg/m^3. Equation (16) is accurate to within $\pm 10\%$ for $0.1<\bar{\alpha}<0.001$ and $0.1\ \text{m}<R_c<1$ m.

The predicted resonant frequencies of the volume mode of oscillation of a 2-D semicircular bubble plume with the bubble radius, $a=1$ mm, are shown plotted directly on the spectrographs of two events in Fig. 15. The top spectrograph is for the 2-D event, packet W_2 with $S=0.448$, and the bottom one is for the 3-D event with $G=0.55$. The predicted resonant frequencies, shown plotted as $\Uparrow$, match closely with the low-frequency spectral peaks for both events. The predicted resonant frequencies of the $n=1$ mode of a semicircular plume with $a=1$ mm are compared to the observed frequencies for all six events in Fig. 16. With the exception of two data points the observed frequencies are all within 30% of the predicted resonant frequencies. The close agreement between the observed low-frequency signals and the theoretically predicted resonant frequencies strongly supports our hypothesis that the observed bubble plumes were oscillating collectively.

VII. DISCUSSION

As stated earlier, because of the finite size of the wave tanks and the long wavelengths of the observed signals, it was necessary to place the hydrophones in the near field of the breaking events. In the near field of a complex acoustic source the observed pressure fluctuations may be due to higher-order poles, the turbulent flow field, the oscillation

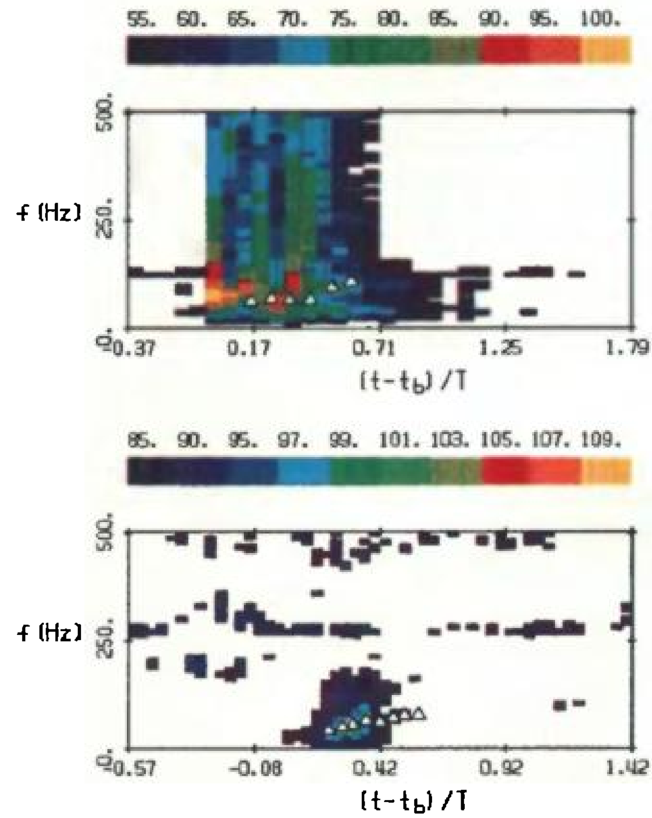

FIG. 15. (Top) Spectrograph of the signal from the microphone for the 2-D breaking event W_2 with $S=0.448$. (Bottom) Spectrograph of the signal from the downstream hydrophone for the 3-D breaking event with $G=0.55$. The predicted resonant frequencies of the $n=1$ mode of a semicylindrical bubble plume with $a=1$ mm are shown marked with Δ. The spectra were averaged over at least three repeats of the event. Each color corresponds to a 2 or 5 dB *re*: 1 μPa^2 increment in pressure spectrum level.

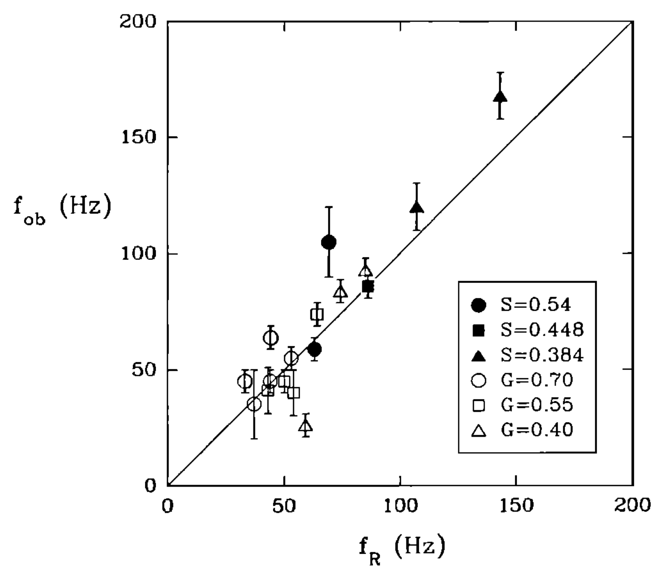

FIG. 16. The frequencies of the observed signals f_{ob} versus the computed eigenfrequencies of the collective volume mode of a semicircular cylindrical plume located at the free surface f_R. The error bars indicate the 3 dB width of the observed spectral peaks. There is more than one point plotted for some events because comparisons were possible at more than one time in these cases.

of individual bubbles, or the collective volume oscillation of the entire plume. The fact that we were able to accurately predict the observed frequencies by assuming the plumes were oscillating collectively in their volume mode, strongly supports our contention that the dominant source of the observed low-frequency signals was the collective volume oscillation of the plumes.

The proximity of the tank boundaries may have an effect on the observed resonant frequencies or eigenfrequencies of the bubble plumes. However experimental and theoretical results indicate that the effect of the tank size on the eigenfrequencies of bubble plumes is very weak.[13,14] In their bubble column experiments, Yoon *et al.*[13] found that the eigenfrequencies did not vary significantly as the ratio of the plume diameter to the tank diameter was varied from 7 to 33. Kolaini *et al.*[14] conducted their bubble plume experiments in two different size tanks for which the ratio of the plume diameter to the tank length scale was equal to 10 and 30. They found that there was a negligible difference between the oscillation frequencies observed in the two tanks. In order to estimate the effect of the proximity of the tank boundaries in our experiments, we computed eigenfrequencies for the 2-D bubble plumes based on two tank sizes. We modeled the wave channel cross section as semicircular in shape and rigid in order to obtain an analytical solution. The details of this derivation can be found in Lu *et al.*[15] Sec. V. We found that the computed eigenfrequencies for a tank of radius 1.0 m and for a tank with an infinite radius varied by 3% or less. Therefore, we concluded that the proximity of the boundaries had a negligible effect on the eigenfrequencies of both the 2-D and 3-D plumes.

The proximity of the tank boundaries will also have an effect on the measurements of the mean-square pressure. Sound generated by the breaking waves will reverberate in the wave tank. Simply stated, this means that the pressure signals radiated by the source will propagate past the receiver more than once as they are reflected off the boundaries of the tank. As a result, the magnitude of the mean-square pressure that we have measured in the wave tanks will be greater than the magnitude that we would have measured if the experiments had been conducted in an infinitely large wave tank (a nonreverberant environment). However for a linear system, the correlations of the mean-square pressure with the fractional dissipation and the gain G (Figs. 4 and 8) will remain qualitatively the same. The magnitudes of the mean-square pressure will be larger than the corresponding free-field values and this will cause the correlation curves to be shifted upward but we do not think this effect altered the trends in the data significantly.

The results from the 2-D experiments indicate that for breaking waves of this scale individual air bubbles oscillating at their resonant frequency are not a significant source of sound at frequencies below approximately 500 Hz. This is consistent with the observations of Medwin and Daniel[6] who found that the largest diameter bubble entrained by gently spilling waves was 14.8 mm which corresponds to a resonant frequency of 440 Hz. Unfortunately, the high levels of background noise in the frequency range 150 Hz to 1 kHz prevented us from determining if this frequency remained the same for the larger scale 3-D breakers. However, we believe that larger scale breaking waves will entrain larger diameter bubbles and therefore the oscillation of individual bubbles may be a significant source of sound at frequencies as low as 200 to 300 Hz under full-scale breakers. It is likely that for full-scale breaking ocean waves there is a frequency range in which both collective plume oscillations and single bubble oscillations are important.

In the 2-D experiments the plunging breakers produced sound at frequencies below 500 Hz and the spilling breakers did not. While this result is attractive because it implies there may be a method for differentiating between spilling and plunging breakers it may not apply to full scale breaking ocean waves. Large-scale spilling breakers may generate thin layers of bubbles at the ocean surface (as opposed to the deeper cylindrical bubble plumes which plunging breakers produce) and it is entirely possible that these bubble layers produce low-frequency sound by oscillating collectively.[15]

The sound spectra of the 3-D breaking events sloped at -5 to -6 dB per octave at frequencies greater than 1 kHz. It has been demonstrated in other studies that at very low windspeeds, or when the breaking waves are small-scale gently spilling breakers, that the spectral slope at frequencies greater than 1 kHz is approximately -5 dB per octave.[5,8] The mechanism responsible for the generation of the sound was shown to be the oscillation of individual air bubbles entrained by the spilling breaking waves. Our results suggest that it is the same sound generation mechanism which produces the higher-frequency sound beneath much larger scale plunging breakers. If this is true, then it may be possible to model the higher-frequency sound generated by both large- and small-scale breaking waves based on the sound radiated by a single bubble oscillating at its linear resonant frequency.[25]

Accurate modeling of the low-frequency sound generated by collective oscillations will require a thorough understanding of the damping of these signals. Our theoretical analysis predicts that the collective volume mode is most heavily damped when the individual air bubbles comprising the plume have a radius equal to 1 mm. The damping is shown to be proportional to the factor (ba^2), the damping constant of an individual bubble, at the resonant frequency of the entire plume, times the square of the bubble radius.

VIII. CONCLUSIONS

We have presented what we believe is the first direct evidence that bubble plumes entrained by unsteady breaking waves generate low-frequency sound by oscillating collectively in their volume mode. Mechanically generated dispersive wave packets were focused to produce energetic plunging and spilling 2-D and 3-D breakers. Low-frequency signals were observed up to $\frac{1}{3}$ of a wave period following the start of active breaking beneath both the 2-D and 3-D breaking events. It was hypothesized that these low-frequency signals were due to the collective volume oscillation of the bubble plumes. To investigate the validity of this hypothesis, theoretical predictions of the resonant frequencies of the volume mode of the observed bubble plumes were made using the void fraction data of Lamarre and Melville[16,17] (for the same experiments), and these values were compared to the frequencies of the observed signals. For all six events the predicted resonant frequency of the lowest mode closely matched the observed frequencies (see Fig. 16). The close agreement between the theoretical predictions and the observations provides strong support for the hypothesis that the bubble plumes were oscillating collectively in their volume mode. Therefore, we conclude that the collective volume oscillations of bubble plumes entrained by breaking waves may be a source of low-frequency sound in the ocean.

ACKNOWLEDGMENTS

We gratefully acknowledge the assistance provided by Peter Johnson and his staff at the Offshore Technology Research Center at Texas A&M University during the 3-D breaking experiments. We wish to thank Eric Lamarre for his collaboration in the 3-D experiments and for extensive discussions of the results. We thank an anonymous reviewer for constructive criticism of the original manuscript. This work was supported by a grant from the Office of Naval Research (Ocean Acoustics).

[1] D. M. Farmer and S. Vagle, "On the determination of breaking wave distributions using ambient sound," J. Geophys. Res. **93**, 3591–3600 (1988).

[2] S. Vagel, "An Acoustical Study of the Upper Ocean Boundary Layer," Ph.D. thesis, University of Victoria and Institute of Ocean Sciences, Victoria, B.C. (1989).

[3] R. Hollett, "Underwater sound from whitecaps at sea," J. Acoust. Soc. Am. Suppl. 1 **85**, S145 (1989).

[4] P. A. Crowther, "Bubble noise creation mechanisms," in *Sea Surface Sound*, edited by B. R. Kerman (Kluwer Academic, Boston, 1988), pp. 131–150.

[5] H. Medwin and M. M. Beaky, "Bubble sources of the Knudsen sea noise spectra," J. Acoust. Soc. Am. **86**, 1124–1130 (1989).

[6] H. Medwin and A. C. Daniel, "Acoustical Measurments of Bubble Production by Spilling Breakers," J. Acoust. Soc. Am. **88**, 408–412 (1990).

[7] H. C. Pumphrey and J. E. Ffowcs Williams, "Bubbles as Sources of Ambient Noise," IEEE J. Oceanic Eng. **15**, 268–274 (1990).

[8] G. E. Updegraff and V. C. Anderson, "Bubble noise and wavelet spills recorded 1 m below the ocean surface," J. Acoust. Soc. Am. **89**, 2264–2279 (1991).

[9] V. O. Knudsen, R. S. Alford, and J. W. Emling, "Underwater ambient noise," J. Mar. Res. **7**, 410–429 (1948).

[10] P. Papanicolaou and F. Raichlen, "Wave and Bubble Characteristics in the Surf Zone," in *Sea Surface Sound*, edited by B. R. Kerman (Kluwer Academic, Boston, 1988), pp. 97–109.

[11] A. Prosperetti, "Bubble-related ambient noise in the ocean," J. Acoust. Soc. Am. **84**, 1042–1054 (1988).

[12] W. M. Carey, J. W. Fitzgerald, and D. G. Browning, "Low Frequency Noise from Breaking Waves," *Natural Physical Sources of Underwater Sound*, edited by B. R. Kerman (Kluwer Academic, Boston, 1993), pp. 277–304.

[13] S. W. Yoon, L. A. Crum, A. Prosperetti, and N. Q. Lu, "An Investigation of the Collective Oscillations of a Bubble Cloud," J. Acoust. Soc. Am. **89**, 700–706 (1991).

[14] A. Kolaini, R. A. Roy, and L. A. Crum, "An investigation of the acoustic emissions from a bubble plume," J. Acoust. Soc. Am. **89**, 2452–2455 (1991).

[15] N. Q. Lu, A. Prosperetti, and S. W. Yoon, "Underwater noise emissions from bubble clouds," IEEE J. Ocean Eng. **15**, 275–281 (1990).

[16] E. Lamarre and W. K. Melville, "Air entrainment and dissipation in breaking waves," Nature **351**, 469–472 (1991).

[17] E. Lamarre and W. K. Melville, "Void-fraction measurements and sound-speed fields in bubble plumes generated by breaking waves," J. Acoust. Soc. Am. **95**, 1317–1328 (1994).

[18] E. S. Chan and W. K. Melville, "Deep-water plunging wave pressures on a vertical plane wall," Proc. R. Soc. London Ser. A **417**, 95–131 (1988).

[19] R. J. Rapp and W. K. Melville, "Laboratory measurements of deep water breaking waves," Philos. Trans. R. Soc. London Ser. A **331**, 735–800 (1990).

[20] M. R. Loewen and W. K. Melville, "Microwave Backscatter and Acoustic Radiation from Breaking Waves," J. Fluid Mech. **224**, 601–623 (1991).

[21] K. W. Commander and A. Prosperetti, "Linear pressure waves in bubbly liquids: Comparison between theory and experiments," J. Acoust. Soc. Am. **85**, 732–746 (1989).

[22] A. Prosperetti, L. A. Crum, and K. W. Commander, "Nonlinear bubble dynamics," J. Acoust. Soc. Am. **83**, 502–514 (1988).

[23] A. E. Ruggles, H. A. Scarton, and R. T. Lahey, "An investigation of the propagation of pressure perturbations in bubbly air/water flows," *First International Multiphase Fluid Transients Symposium*, edited by H. H. Safwat, J. Braun, and U. S. Rohatgi (Am. Soc. Mech. Eng., New York, 1986), pp. 1–9.

[24] W. M. Carey, J. W. Fitzgerald, E. C. Monahan, and Qin Wang, "Measurement of the sound produced by a tipping trough with fresh and salt water," J. Acoust. Soc. Am. **93**, 3178–3192 (1993).

[25] M. R. Loewen and W. K. Melville, "A model of the sound generated by breaking waves," J. Acoust. Soc. Am. **90**, 2075–2080 (1991).